Hall A Line of Sight Shielding

K.A.Aniol,CSULA and CEBAF, and V.Punjabi, NSU

Abstract

The effect of line of sight shielding(LOSS) on pion,proton,and neutron induced background is considered for Hall A. FLUKA calculations show that about 75CM LOSS will reduced energetic charged particle fluxes to the level of 7KHz-10KHz in a $1m^2$ region placed in the detector package for a Hall A spectrometer. Further increasing the line of sight shielding does not lower the charged particle rate because the rate is then dominated by particles which strike the hut and miss the LOSS. Placing additional shielding of about 40cm thickness on both sides of the LOSS to shield the hut walls can bring the charged particle rate in the sensitive region of the detector package to about 1KHz-2KHz per $1m^2$.

Introduction

Experience at other high energy electron laboratories has shown the need to place line of sight shielding(LOSS) between targets and detector packages installed in detector huts. This is particularly important at forward angles, and the most serious source of background comes from muons created in the decay of pions in flight. This technical note considers the line of sight shielding needs in Hall A by using realistic pion electroproduction yields and by tracing the history of pions using the hadronic cascade code "FLUKA". The rates due to proton and neutron electroproduction are also calculated in the same fashion. The version of FLUKA employed is that described in CEBAF TN-90-238(by San Jin).

The detector hut geometry as presently envisaged is shown in Figure 1. The hut is a multilayered structure composed of iron,lead,concrete, and boron. A slightly simpler geometry was used in the FLUKA simulations, although the composition was retained. FLUKA has a combinatorial geometry package that facilitates the modelling of geometries. A sketch of the geometry used is shown in Figures 2A and 2B. In all the calculations described here the detector hut geometry/compostion remained fixed and only the LOSS(region 7 - R7) and the EARS(regions 14 and 15 - R14,R15) were varied. The region numbers in Figures 2A and 2B(R1 TO R15) are regions used by FLUKA and they correspond to:

R1	50cm Fe front face and 25.5cm side walls of hut
R2	2.5cm Boron shell in hut
R3	10cm Pb shell in hut
R4	interior of hut,assigned to be air
R5	46cm×212cm polarimeter detector in correct position, assumed to be air
R6	65cm concrete floor of hut
R7	line of sight shielding made of Fe,variable thickness, 90cm wide, and 385cm tall
R8	hall A assumed to be air
R9	black hole which surrounds entire system
R10	50cm×200cm detector in focal plane,assumed to be air
R11	100cm×600cm region of air to monitor particle flux outside of LOSS shadow

R12	100cm×600cm region of air to monitor particle flux in the LOSS shadow
R13	100cm×600cm region of air to monitor particle flux outside the LOSS shadow
R14	84cm×385cm Fe EAR of variable thickness
R15	84cm×385cm Fe EAR of variable thickness

A sample input file for FLUKA for this geometry is presented in Table 1.

For most of the calculations it was assumed that the detector hut, actually the center of the polarimeter detector,R5, made an angle of 24.0 degrees with respect to the electron beam. This is the smallest angle that R5 could be at and it corresponds to the spectrometer being at 0 degrees. A typical forward spectrometer position of 12.5 degrees corresponds to R5 being at 27.3 degrees. A rather high luminosity target was assumed for this modelling, 15cm ^{4}He, 0.17g/cm^3 and 200μA of beam. The pion yield, which includes both direct electroproduction and bremsstrahlung induced photoproduction was calculated with the interactive code CB5B0:[ANIOL]EPRODT2.*. Pion spectra calculated by this code are shown in Figure 3 for different angles. Proton and neutron electroproduction was calculated with the O'Connell-Lightbody code EPC(Figures 8 and 13).

Results

FLUKA does not track particles below 50 MeV kinetic energy. In the results quoted below we will discuss particle fluxes above 50 MeV kinetic energy. For high energy particles the dynamics and kinematics of free hadron-hadron interactions is approximately that of hadron-bound hadron interactions. In this energy regime all shielding that presents the same number of nucleons per unit area has the same effect. We calculated the effect of using concrete for shielding and found that FLUKA ,not surprisngly, gives the same results as for iron, provided the same mass/unit area was used. The advantage in using hydrogenous shielding to degrade the neutron energy is only realized for lowish energy neutrons. Since the line of sight shielding is needed to shadow the detector hut against direct production from the target, there is no shielding advantage in the use of hydrogenous material. Low energy neutrons will be coming from many directions and therefore the most effective position for hydrogenous matterial is at the detector hut itself. The choice of material for the LOSS can therefore be made based on space and cost considerations.

The background due to pion, neutron, or proton electroproduction is described as follows supposing we are discussing the pion contribution. The particle rate into any particular region depends upon the probablity of a pion leaving the target and generating a penetrating particle times the number of pions leaving the target. FLUKA gives, for example for muons, the transmission probability dN_μ/dN_π. The electroproduction code gives the pion yield per electron per unit momentum per sterradian. The muon rate is therefore,

$$\frac{dN_\mu}{dt} = \phi_e \Delta\Omega \int_0^{p_{\pi max}} \frac{dN_\mu}{dN_\pi} \frac{dN_\pi}{dN_e dp_\pi d\Omega} dp_\pi,$$

with

$$\phi_e = 1.25 \times 10^{15} s^{-1},$$

for 200μA and

$$\Delta\Omega = 0.073 Sr,$$

to illuminate the entire front face of the hut.

In Figure 4, as an example of the transmission probability, the ratio of numbers of muon per pion that arrive at R5 as a function of initial pion momentum is plotted for different thicknesses of the line of sight shielding, without the EARS(R14 and R15 were assigned as air). In each case 40000 pions were sent into the solid angle corresponding to the front of the hut as viewed by the target. When a symbol appears to be missing it is because fewer than one muon arrived at R5 in the simulation. The statistical fluctuation is evident in the figure, for example, between 1.0 and 2.0 GeV/c for a shield thickness of 112.5cm. Using the calculations from Figures 3 and 4 it is possible to determine the total charged particle rate to R5, as done in Figure 5. For this calculation the rate due to π^+ alone was doubled to account for π^- induced background. The rates in R5 and R10 are plotted. It is evident that FLUKA predicts a non-homogeneous spatial distribution of the particle fluxes inside the hut. Although R10 is closer to the front of the hut than R5, its solid angle as seen from the target is smaller. Also shown in Figure 5 is the effect of spectrometer angle on the count rate. The extreme forward angle case has a count rate 2-3 times bigger than the rate expected at $\theta_{sp} = 12.5$ deg . The calculation shows that there is a saturation in the background rate that comes in above around 60cm of LOSS(R7). The minimum charged particle count rate in the 1m^2 detector at R5 is 7KHz to 10KHz for the conditions shown. This indicates that detectors in the shadow of the LOSS are susceptible to events generated outside the shadow. The shield house walls are not thick enough to stop all particles generated by pions hitting them. Pions that miss R7 but go through R14 or R15 have a long flight path and contribute to muon production over the full 18.2 m flight path to the hut front face. The effect of placing shielding in R14 and R15 was calculated for different thicknesses of the EARS. These are shown in Figure 6 . There is a definite reduction in the muon transmission probability for the lower pion momenta. No muons were detected in the simulation for 40000 pions at any momentum below 2GeV/c when 40 cm EARS are used. This is good for the shielding since the electroproduction spectra are largest for the smaller momenta.

It will be recognized that R5 or R10 are rather small objects in a large box. The detector package also enjoys the advantage of being in the shadow of the LOSS. However, even with 40cm thick EARS(R14 and R15), a large total rate of particles enters the hut. This should be kept in mind when placing other apparatus inside the hut and outside the LOSS shadow. A series of FLUKA runs were made to estimate the particle fluxes in other areas of the hut. Regions R11,R12, and R13 were defined to be 1mX6m and placed near the front wall of the hut. They were assigned to be air so they had minimal effect on the particle transport inside the hut. The entire hut inner space R4 was also scored for particle fluxes so that an estimate could be made of the total flux entering the hut. The FLUKA runs were made with R7 fixed at 75cm thickness of Fe, and the EARS thicknesses were varied. Tables 2,3,4 lists the separate particle rates for π, μ ,protons, and neutrons in R5,R10,R11+R13,R12, and R4. From these tables it can be expected that we might achieve a factor of 2 to 10 reduction in the energetic charged particle flux at R5 giving

a rate of about 1KHz-2KHz for $1m^2$ with 40cm thick EARS. The spectrum of particles entering the hut(R4) for incident π^+ only is shown in Figure 7. We include in Figures 8-17 data used for background calculations from electroproduced protons and neutrons.

The total neutron flux (E > 50MeV) from all sources entering the hut is about $2.5Ms^{-1}$. The neutrons generate charged particle events via nuclear interactions. Using a realisitic value of $\sigma_{tot} = 0.35$barns for A = 12, the neutron induced count rate in a 1 m^2 scintillator is less than $100s^{-1}$ and in the entire hut about $35Ks^{-1}$.

Calculations were also performed to investigate the line of sight rate due to the electron beam passing through the helium gas bag. In this case there is no LOSS to shadow the hut. The transmission probability of muons per pion naturally increases, but when all the factors are taken into account, e.g., increased angle of observation and lower density of gas, the direct line of sight rate due to the gas bag is about 1 % of that due to the target with 75 cm thick LOSS in place.

Summary

FLUKA calculations show that about 75CM LOSS will reduced energetic particle fluxes to the level of 7KHz-10KHz in a $1m^2$ region placed in the detector package for a Hall A spectrometer. Further increasing the line of sight shielding does not lower the charged particle rate because the rate is then dominated by particles which strike the hut and miss the LOSS. Placing additional shielding adjacent to the LOSS of about 40cm thickness to shield the hut walls can bring the rate in the sensitive region of the detector package to about 1KHz-2KHz per $1m^2$.

TABLE 1 Input file for Hall A line of sight shielding calculations. FLUKA calculations

```
TITLE
DETECTOR HUT,HALL A,2.5GEV PION,XB = 0,12.5 DEG,75CM L.O.S.S.,40CM EARS
BEAM       2.50        0.0         270.        0.0         0.0         1.0         PION+
BEAMPOS    0.1         0.1         0.1         0.899       0.391       0.0
DISCARD    5.0         6.0         0.0         0.0         0.0         0.0
GEOBEGIN   0.0         0.          0.0         0.          0.          0.0         COMBINAT
    0     0
  BOX      1       1834.        531.       147.6        805.          0.        179.
                      0.        825.          0.       -110.          0.        495.
  BOX      2       1877.        596.       184.0         731.          0.        163.
                      0.       734.5          0.         -99.          0.        445.
  BOX      3     1878.5         598.5      185.9         726.          0.        162.
                      0.       729.5          0.         -98.          0.        440.
  BOX      4     1886.6         608.5      197.6         707.          0.        157.
                      0.       709.5          0.         -94.          0.        421.
  BOX      5     2535.0        1000.0      539.0         1.38       1.41         0.31
                 -146.4         149.9      -32.4         -9.9          0.        44.9
  BOX      6     1834.0         531.0      147.6         805.          0.        179.
                      0.          65.          0.       -110.          0.        495.
  BOX      7      948.9         192.0      164.2         73.2          0.        16.4
                      0.         385.          0.        -19.5          0.        87.9
  BOX      8        0.            0.          0.       3000.0          0.          0.
                      0.       3000.0          0.          0.          0.       3000.0
  BOX      9      2092.         771.0       438.0      195.30          0.        43.3
                      0.           5.          0.        -10.8          0.        48.8
  BOX     10     1879.7         618.5       254.1        0.97          0.        0.22
                      0.         600.0          0.       -21.6          0.        97.6
  BOX     11     1856.0         618.5       360.8        0.97          0.        0.22
                      0.         600.0          0.       -21.6          0.        97.6
  BOX     12     1832.4         618.5       467.1        0.97          0.        0.22
                      0.         600.0          0.       -21.6          0.        97.6
  BOX     13      970.0         192.0        75.0        39.0          0.        8.64
                      0.         385.0          0.       -18.2          0.        82.0
  BOX     14      925.0         192.0       260.0        39.0          0.        8.64
                      0.         385.0          0.       -18.2          0.        82.0
  END
  R01     0      +1      -2      -6
  R02     0      +2      -3
  R03     0      +3      -4
  R04     0      +4      -5      -9      -10      -11      -12
  R05     0      +5
  R06     0      +6
  R07     0      +7
  R08     0      +8      -1      -7      -13      -14
  R09     0      -8
  R10     0      +9
  R11     0     +10
  R12     0     +11
  R13     0     +12
  R14     0     +13
  R15     0     +14
  END
GEOEND
SCORE      13.         10.0        1.0         8.0         0.0         0.
MATERIAL   5.          10.8        2.34        26.                               BORON
ASSIGNMA   11.         1.          1.          1.          0.          0.
ASSIGNMA   26.         2.          2.          1.          0.          0.
ASSIGNMA   17.         3.          3.          1.          0.          0.
ASSIGNMA   24.         4.          4.          1.          0.          0.
ASSIGNMA   24.         5.          5.          1.          0.          0.
ASSIGNMA   25.         6.          6.          1.          0.          0.
ASSIGNMA   11.         7.          7.          1.          0.          0.
ASSIGNMA   24.         8.          8.          1.          0.          0.
ASSIGNMA   1.          9.          9.          1.          0.          0.
ASSIGNMA   24.         10.         13.         1.          0.          0.
ASSIGNMA   11.         14.         15.         1.          0.          0.
CALOR      5.          5.          1.          0.05        0.          0.
OUTLEVEL   1.0         4.0         0.0         0.0         0.0         0.0
BOUNDARY   4.          5.          10000.      4.          10.         10000.      CURRENT1
BOUNDARY   8.          7.          28875.      3.          4.          2264173.    CURRENT1
BOUNDARY   4.          11.         60000.      4.          13.         60000.      CURRENT1
BOUNDARY   4.          12.         60000.                                          CURRENT1
THRESHOL   0.05        0.0         0.0         0.0         0.0         0.0
ENERBINS   0.10        0.10        0.10        0.0         0.0         0.0         LINEAR
START      40000.      10000000.   0.          0.          0.          0.
STOP
```

Table 2

Rates† due to π^+ for various regions as a function of EARS thickness
LOSS kept at 75cm Fe

region	EARS (cm)	μ (s^{-1})	π (s^{-1})	p (s^{-1})	n (s^{-1})	$2\times(\pi+\mu+\text{p})$ (s^{-1})
R5	0.	3.7K	1.6K	<100	12.4K	10.6K
	20.	1.2K	<100	<100	2.3K	2.6K
	40.	550	<100	<100	4.0K	1.1K
R10	0.	1.6K	1.1K	280	7.1K	6.0K
	20.	110.	<100	<100	850.	200.
	40.	170.	<100	<100	1.2K	400.
R11+R13	0.	1236K	197K	3.6K	720K	2874K
	20.	450K	59K	710	202K	1020K
	40.	340K	46K	1.5K	160K	774K
R12	0.	10.6K	600	<100	13.8K	22.4K
	20.	8.7K	1.2K	<100	26.1K	19.8K
	40.	8.2K	800	<100	15.6K	16K
R4	0.	2015K	414K	10.3K	1290K	4879K
	20.	679K	79.2K	3.6K	362K	1524K
	40.	430K	51K	1.9K	217K	966K

† - Assuming 200μA electron beam on a 2.55g/cm^2 ^{4}He target at maximum forward spectrometer angle.

Table 3

Rates† due to protons for various regions as a function of EARS thickness
LOSS kept at 75cm Fe

region	EARS (cm)	p (s^{-1})	n (s^{-1})	$\pi + \mu$ (s^{-1})
R5	0.	<100	6.9K	<100
	20.	<100	6.1K	<100
	40.	<100	1.1K	<100
R10	0.	<100	8.1K	<100
	20.	<100	2.4K	<100
	40.	<100	5.0K	<100
R11+R13	0.	9.9K	440K	128
	20.	2.4K	170K	<100
	40.	2.3K	120K	<100
R12	0.	<100	7.1K	<100
	20.	<100	2.4K	<100
	40.	<100	2.7K	<100
R4	0.	17K	840K	177
	20.	2.9K	290K	<100
	40.	4.7K	210K	<100

† - Assuming 200μA electron beam on a 2.55g/cm^2 ^{4}He target at maximum forward spectrometer angle.

Table 4

Rates† due to neutrons for various regions as a function of EARS thickness
LOSS kept at 75cm Fe

region	EARS (cm)	p (s^{-1})	n (s^{-1})	$\pi + \mu$ (s^{-1})
R5	0.	560	88K	<100
	20.	163	36K	<100
	40.	<100	32K	<100
R10	0.	130	52K	<100
	20.	<100	33K	<100
	40.	<100	25K	<100
R11+R13	0.	43K	3800K	809
	20.	14K	1900K	563
	40.	8.1K	1300K	<100
R12	0.	973	140K	<100
	20.	<100	260K	<100
	40.	<100	180K	<100
R4	0.	92K	7500K	1.3K
	20.	26K	3600K	801
	40.	10K	2100K	<100

† - Assuming 200μA electron beam on a 2.55g/cm^2 ^{4}He target at maximum forward spectrometer angle.

FIGURE 1 HALL A DETECTOR HUT

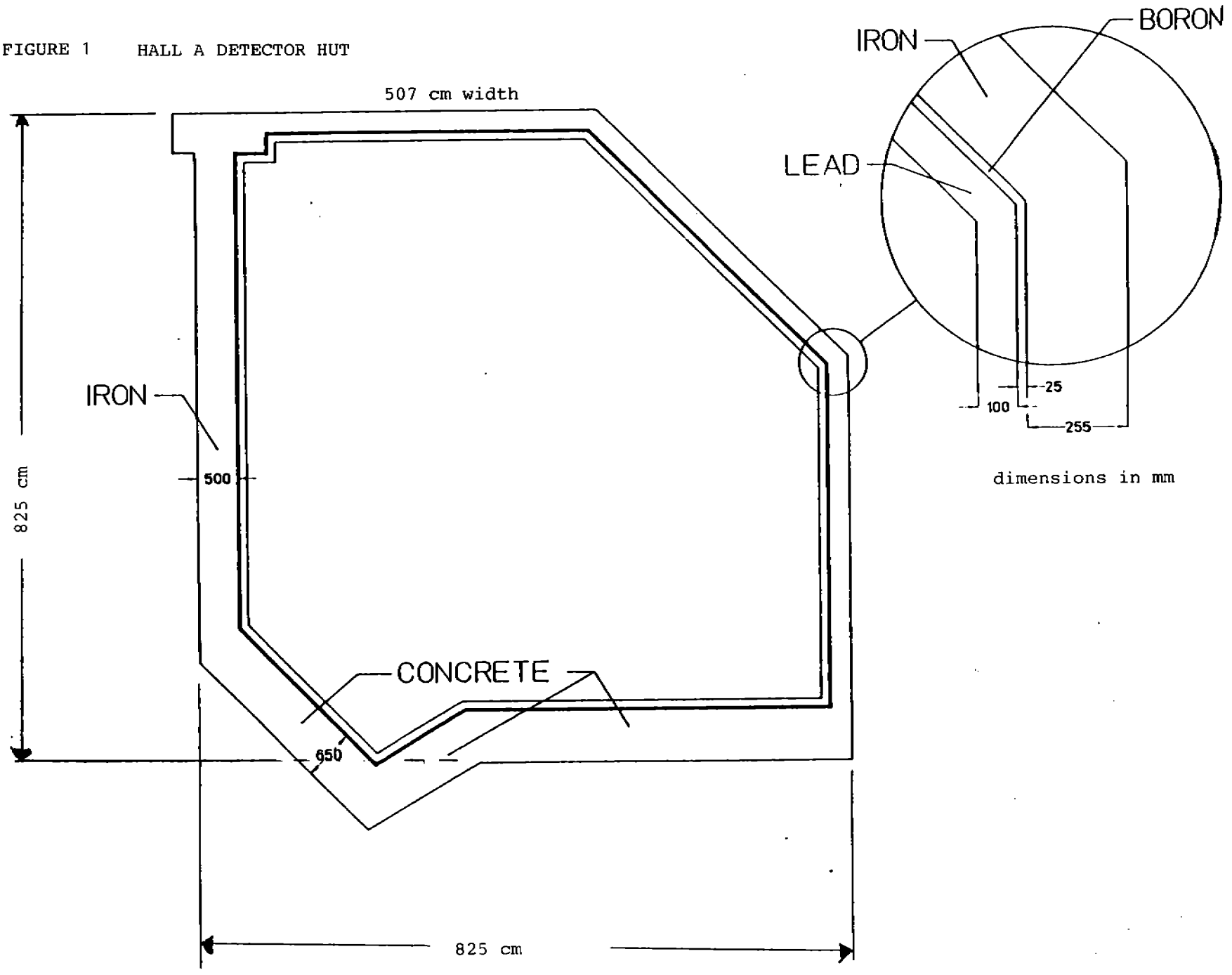

FIGURE 2A HALL A DETECTOR HUT MODEL, TOP VIEW

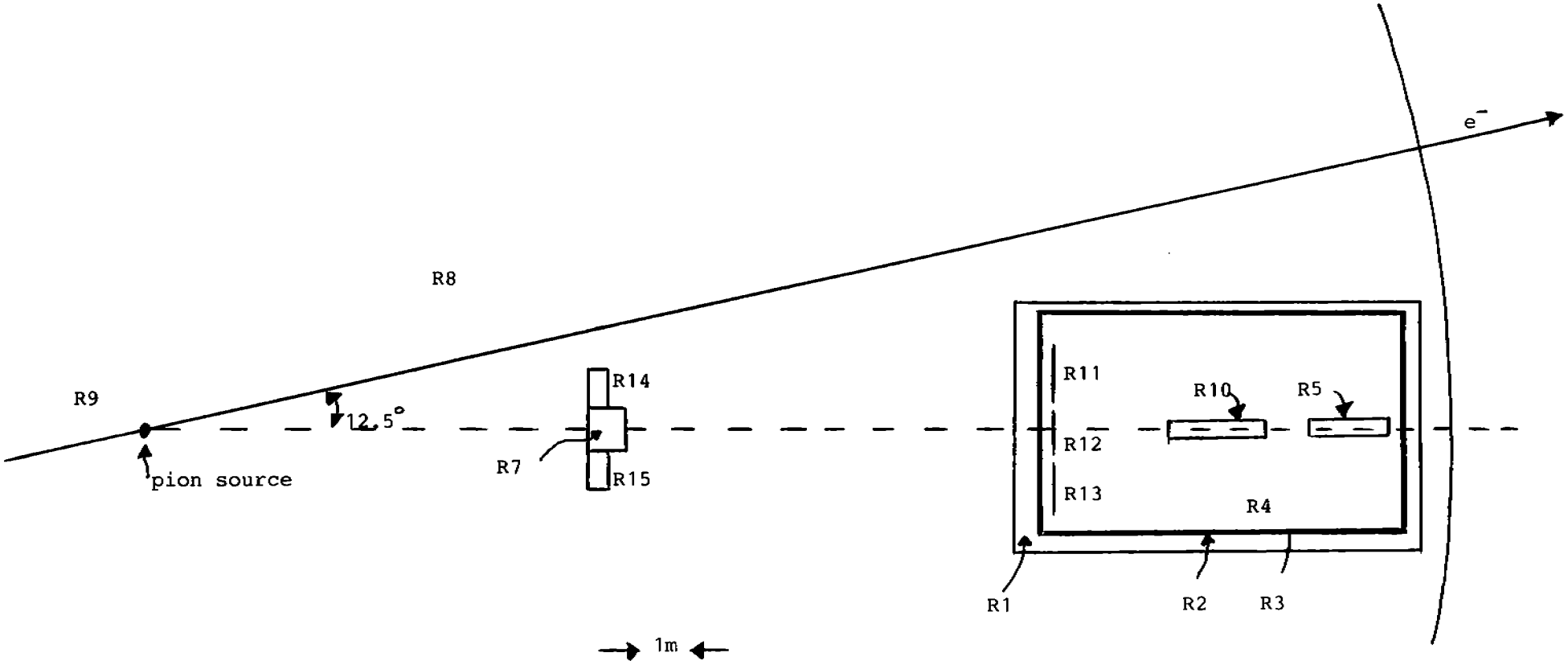

FIGURE 2B HALL A DETECTOR HUT MODEL, SIDE VIEW

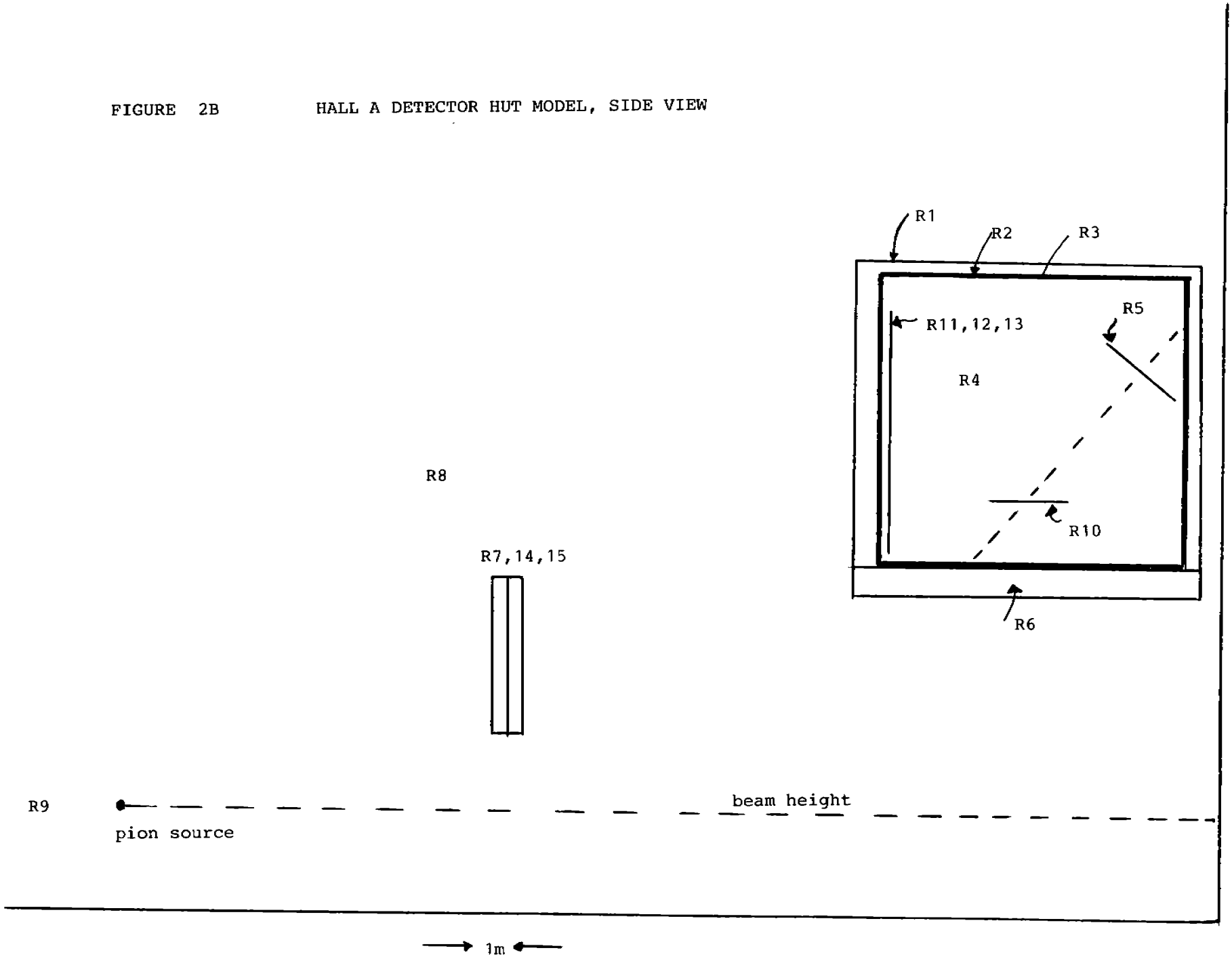

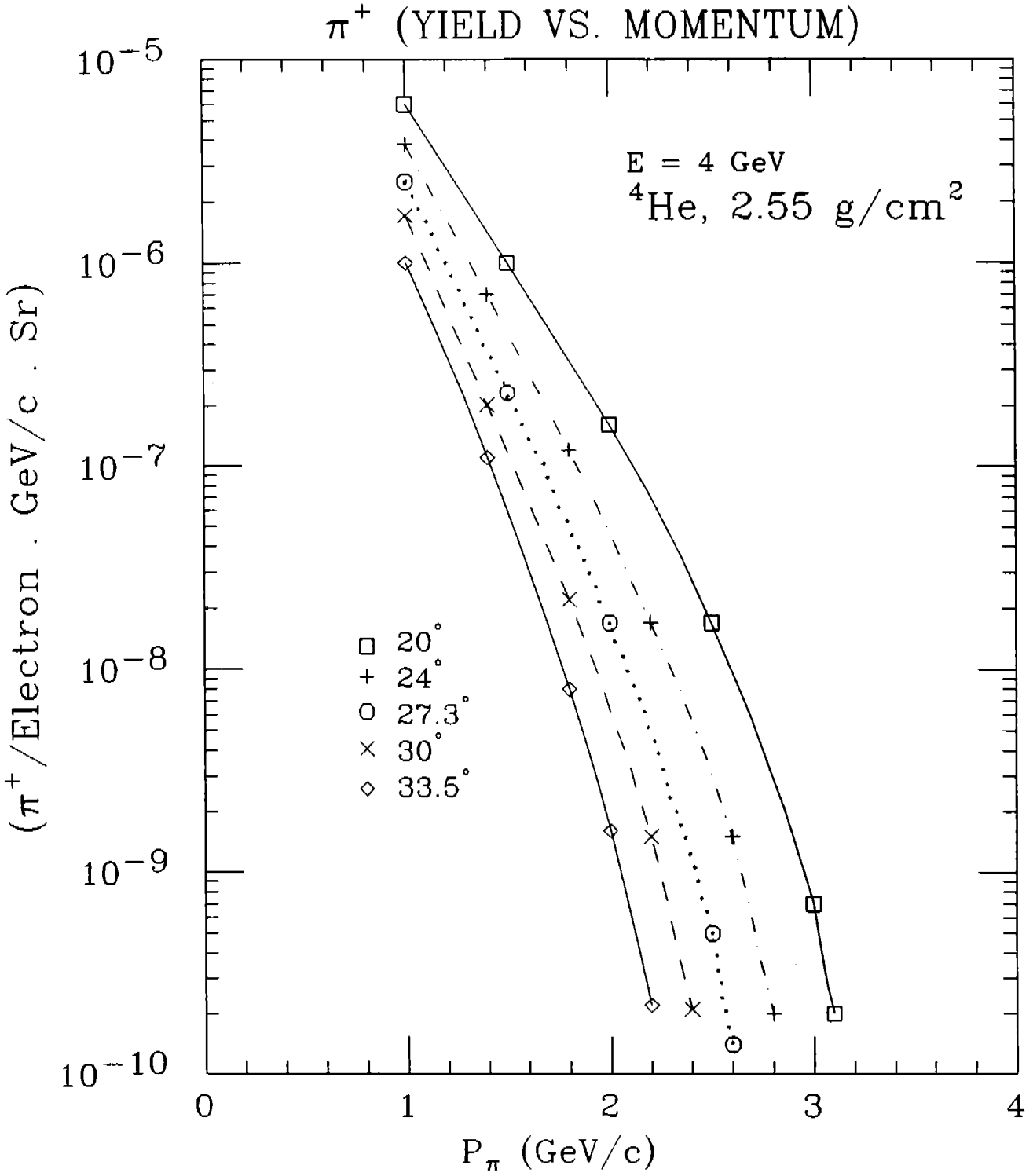
π^+ (YIELD VS. MOMENTUM)
E = 4 GeV
^{4}He, 2.55 g/cm^2
20°
24°
27.3°
30°
33.5°
$(\pi^+/\text{Electron} \cdot \text{GeV/c} \cdot \text{Sr})$
10^{-5}
10^{-6}
10^{-7}
10^{-8}
10^{-9}
10^{-10}
0
1
2
3
4
P_π (GeV/c)

Figure 3

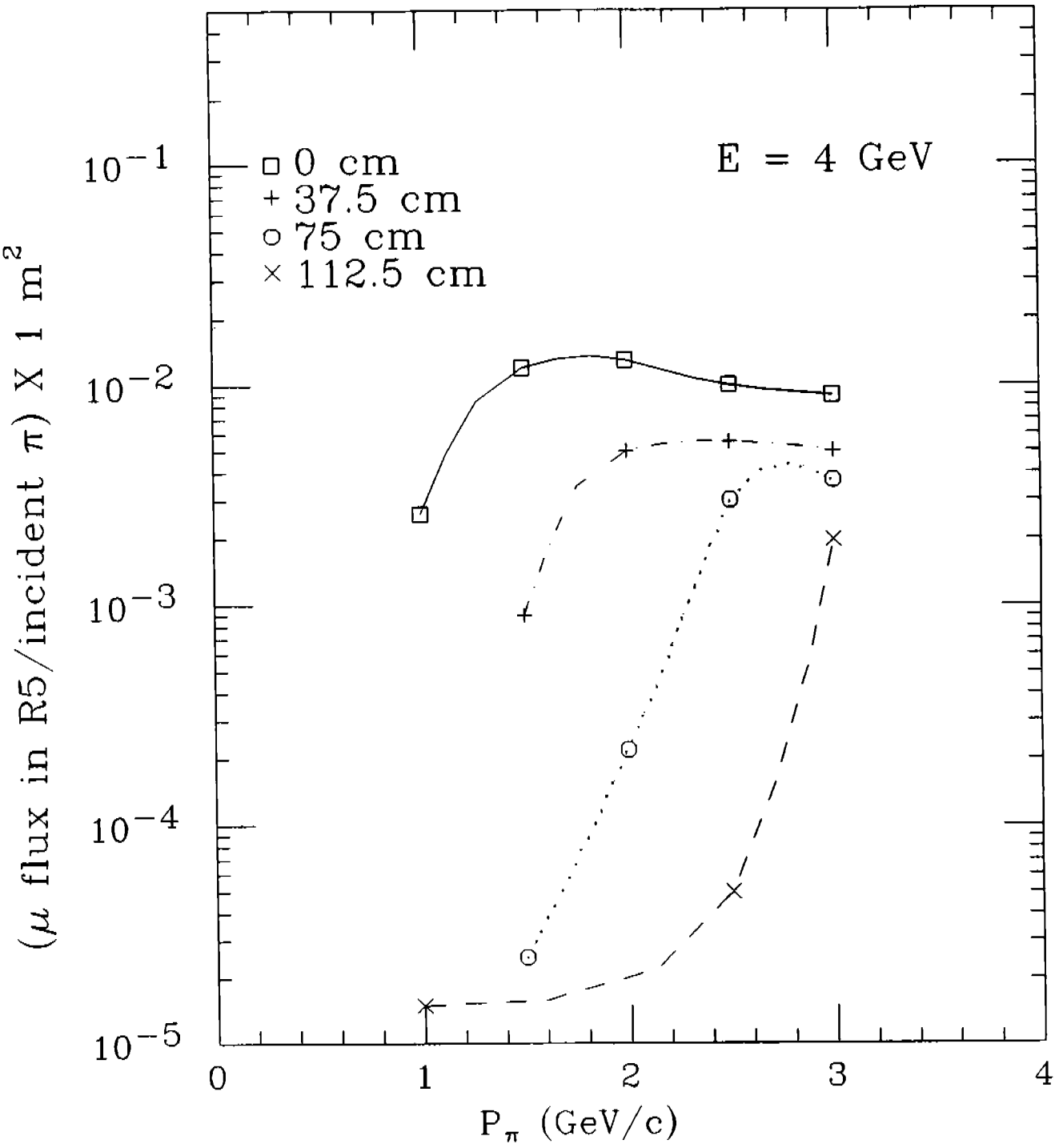
E = 4 GeV
□ 0 cm
+ 37.5 cm
○ 75 cm
× 112.5 cm
10^{-1}
10^{-2}
10^{-3}
10^{-4}
10^{-5}
0
1
2
3
4
(μ flux in R5/incident π) X 1 m^2
P_π (GeV/c)

Figure 4

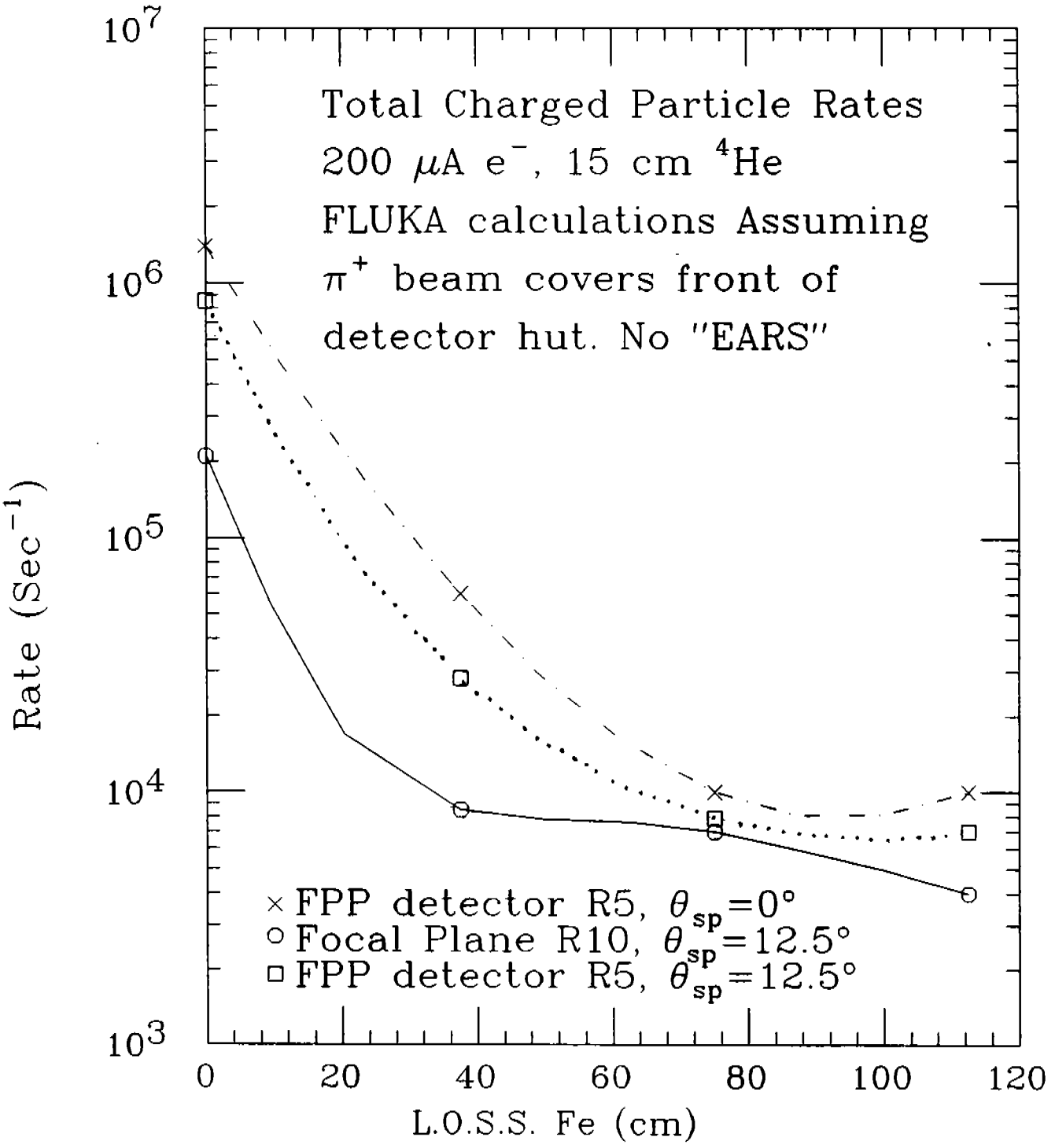
Total Charged Particle Rates
200 μA e⁻, 15 cm ⁴He
FLUKA calculations Assuming
π⁺ beam covers front of
detector hut. No "EARS"
× FPP detector R5, θsp=0°
○ Focal Plane R10, θsp=12.5°
□ FPP detector R5, θsp=12.5°
Rate (Sec⁻¹)
10⁷
10⁶
10⁵
10⁴
10³
0
20
40
60
80
100
120
L.O.S.S. Fe (cm)

Figure 5

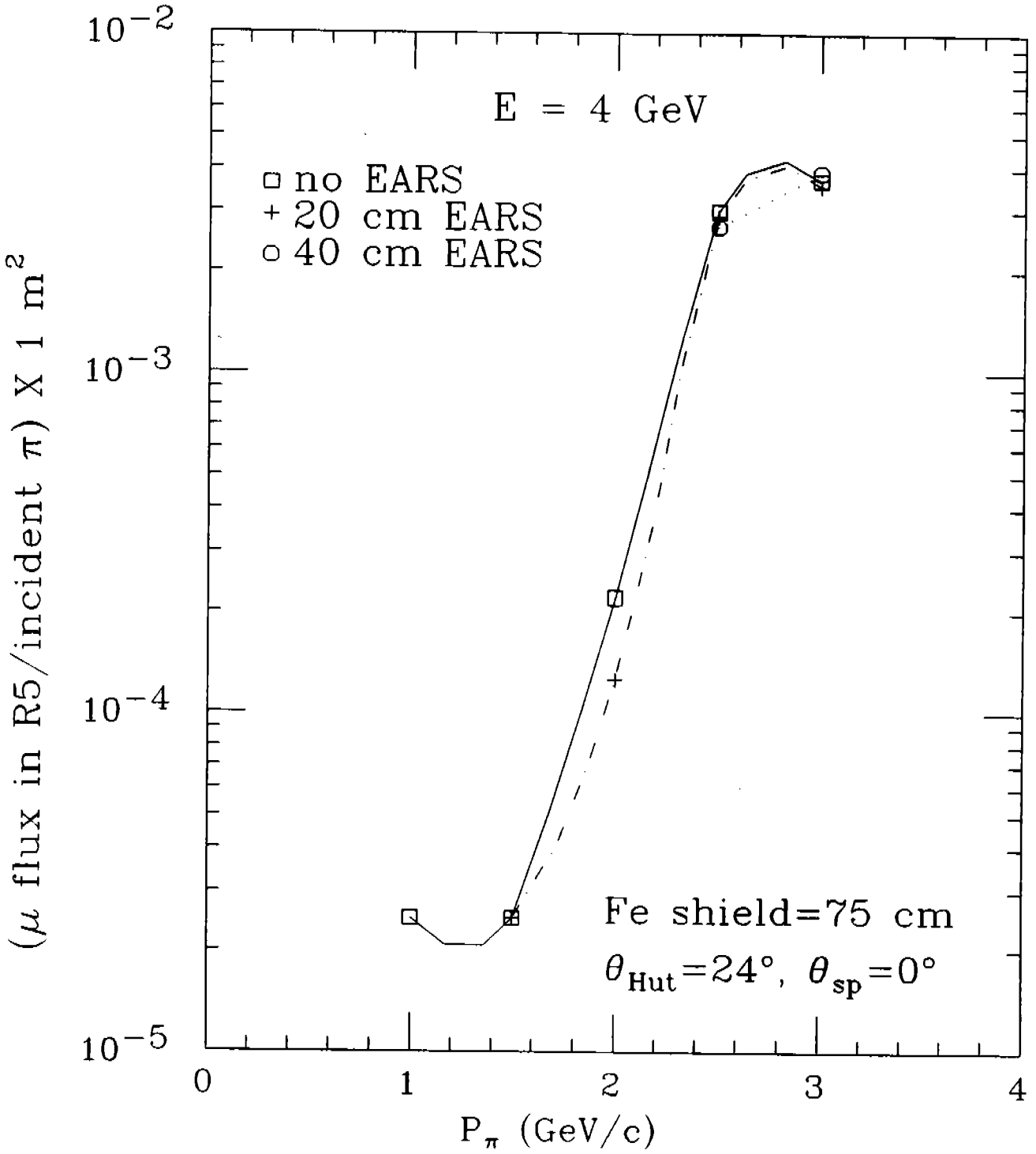
E = 4 GeV
no EARS
20 cm EARS
40 cm EARS
Fe shield=75 cm
θ_{Hut}=24°, θ_{sp}=0°
10^{-2}
10^{-3}
10^{-4}
10^{-5}
0
1
2
3
4
(μ flux in R5/incident π) X 1 m^2
P_π (GeV/c)

Figure 6

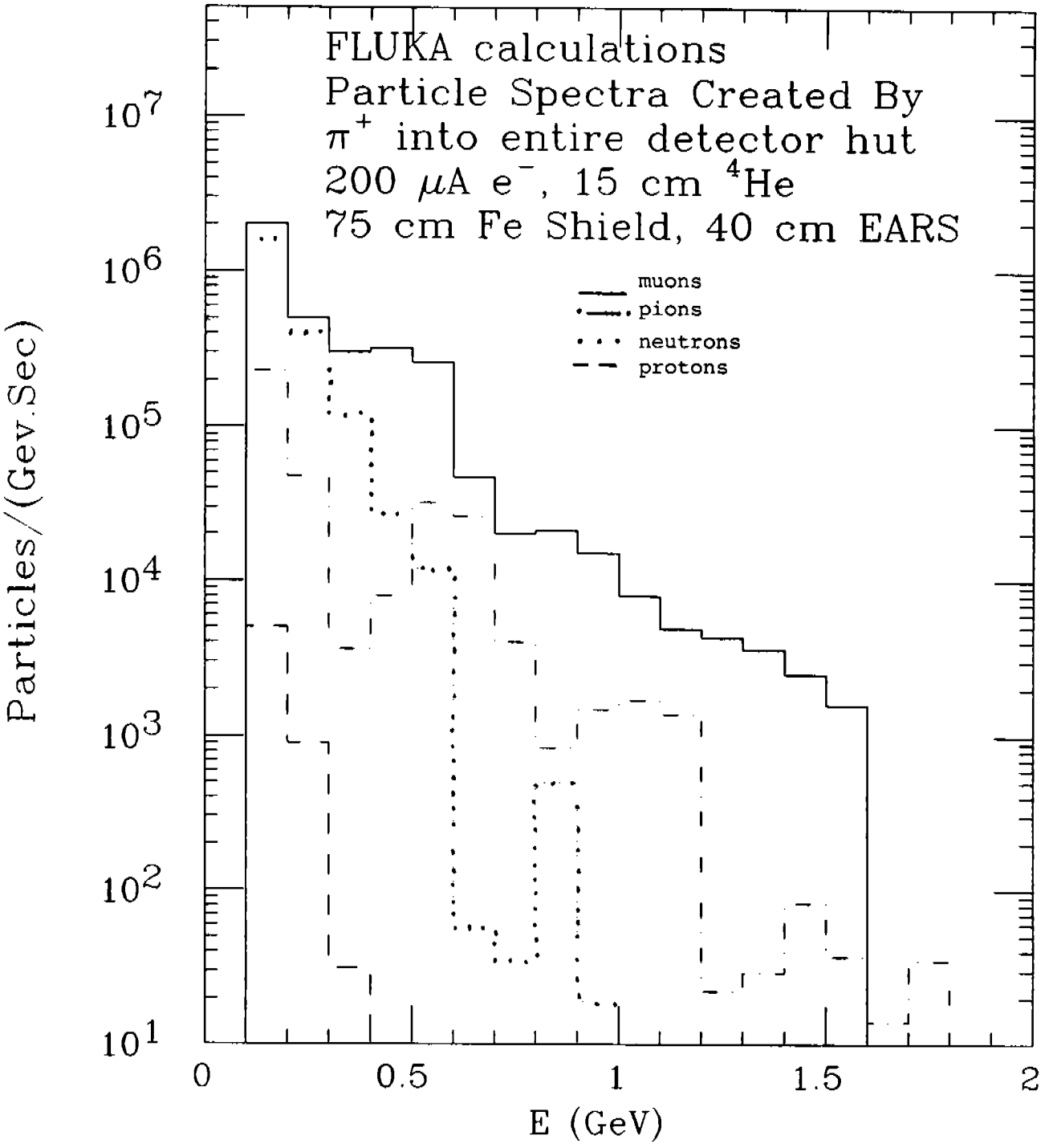
FLUKA calculations
Particle Spectra Created By
π^+ into entire detector hut
200 μA e^-, 15 cm ^{4}He
75 cm Fe Shield, 40 cm EARS
muons
pions
neutrons
protons
Particles/(Gev.Sec)
10^7
10^6
10^5
10^4
10^3
10^2
10^1
0
0.5
1
1.5
2
E (GeV)

Figure 7

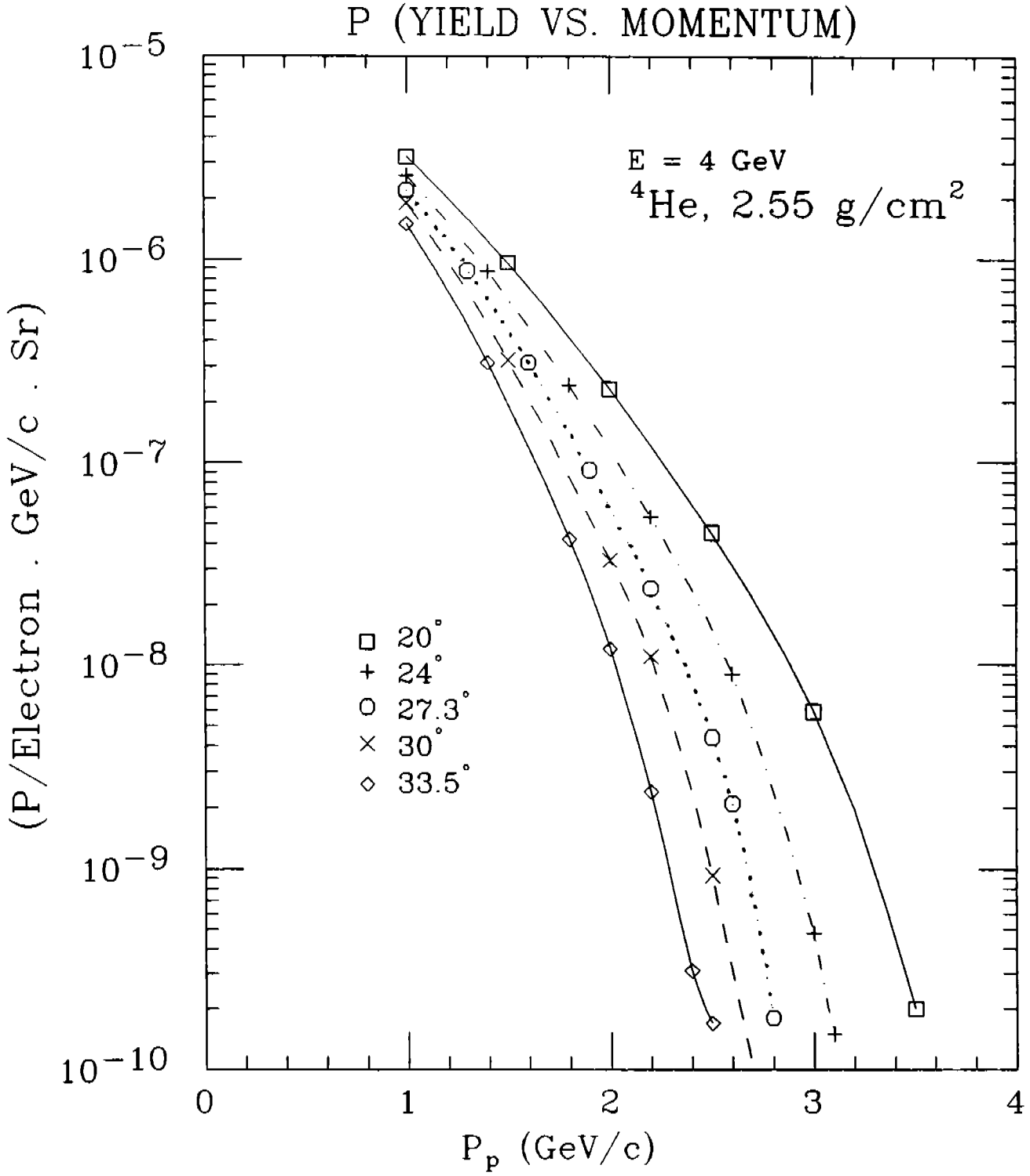
P (YIELD VS. MOMENTUM)
E = 4 GeV
^{4}He, 2.55 g/cm^2
20°
24°
27.3°
30°
33.5°
(P/Electron . GeV/c . Sr)
P_p (GeV/c)
10^{-5}
10^{-6}
10^{-7}
10^{-8}
10^{-9}
10^{-10}
0
1
2
3
4

Figure 8

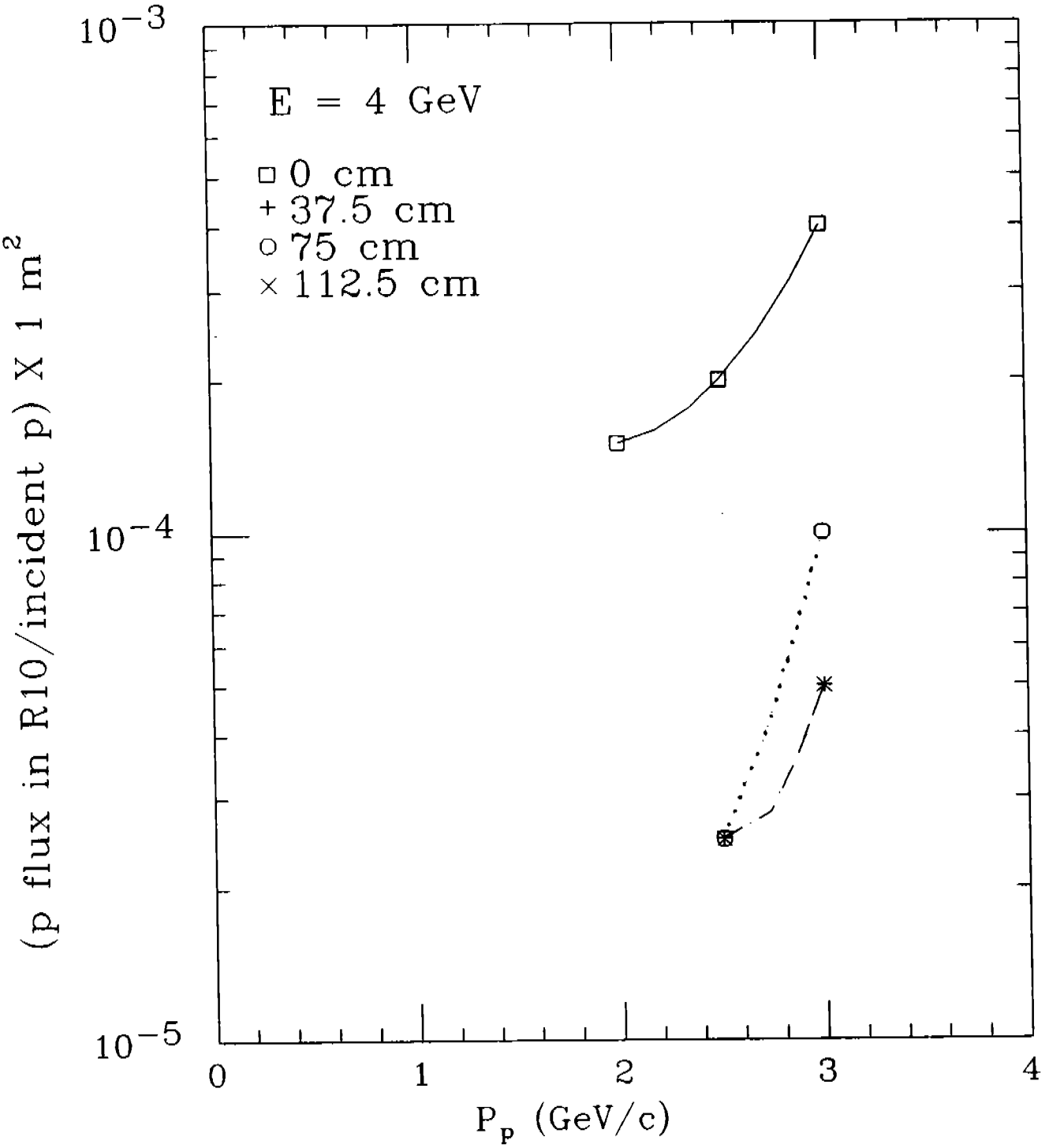
E = 4 GeV
□ 0 cm
+ 37.5 cm
○ 75 cm
× 112.5 cm
10^{-3}
10^{-4}
10^{-5}
0
1
2
3
4
P_p (GeV/c)
(p flux in R10/incident p) X 1 m^2

Figure 9

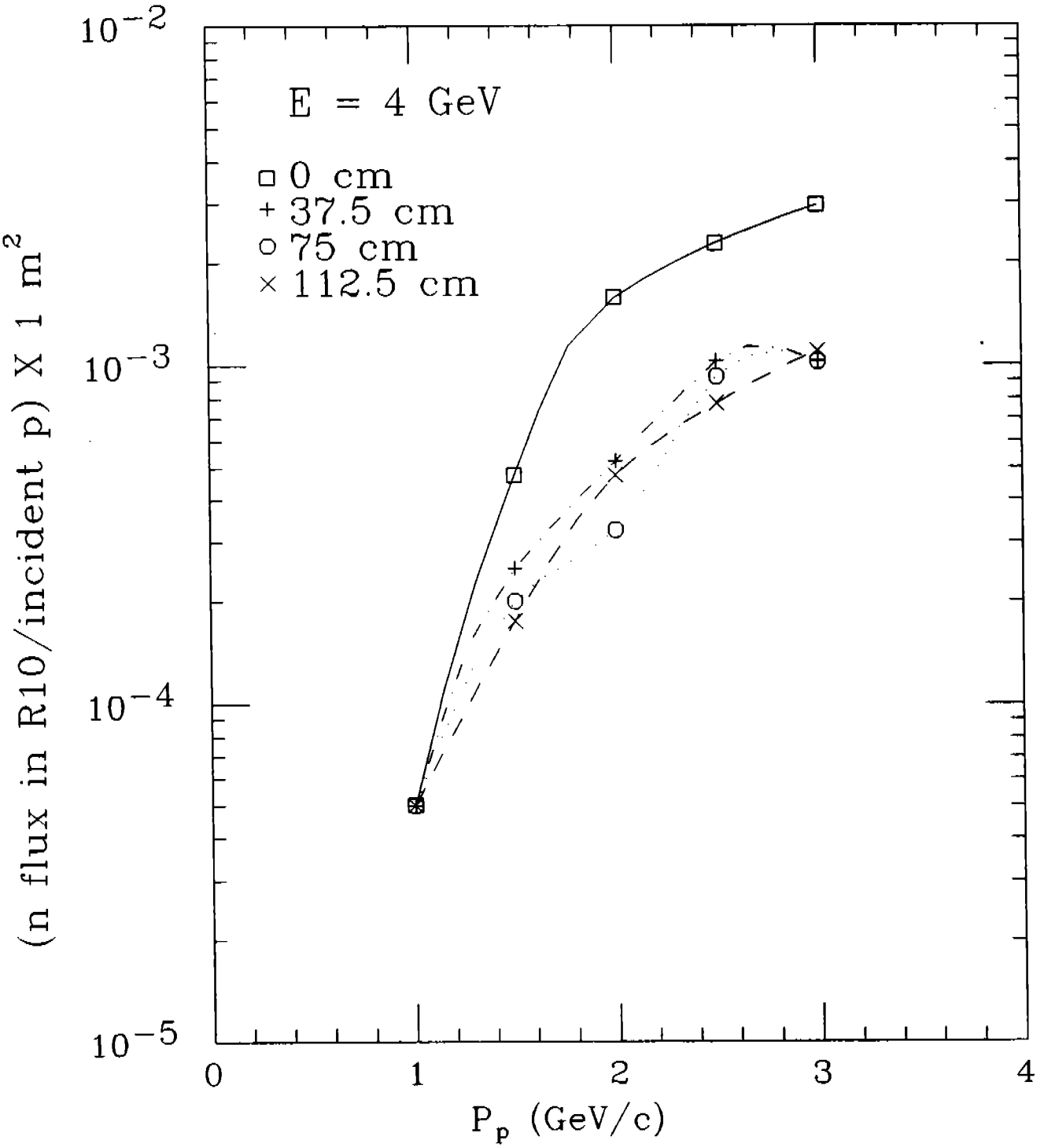
E = 4 GeV
0 cm
37.5 cm
75 cm
112.5 cm
(n flux in R10/incident p) X 1 m^2
10^{-2}
10^{-3}
10^{-4}
10^{-5}
0
1
2
3
4
P_p (GeV/c)

Figure 10

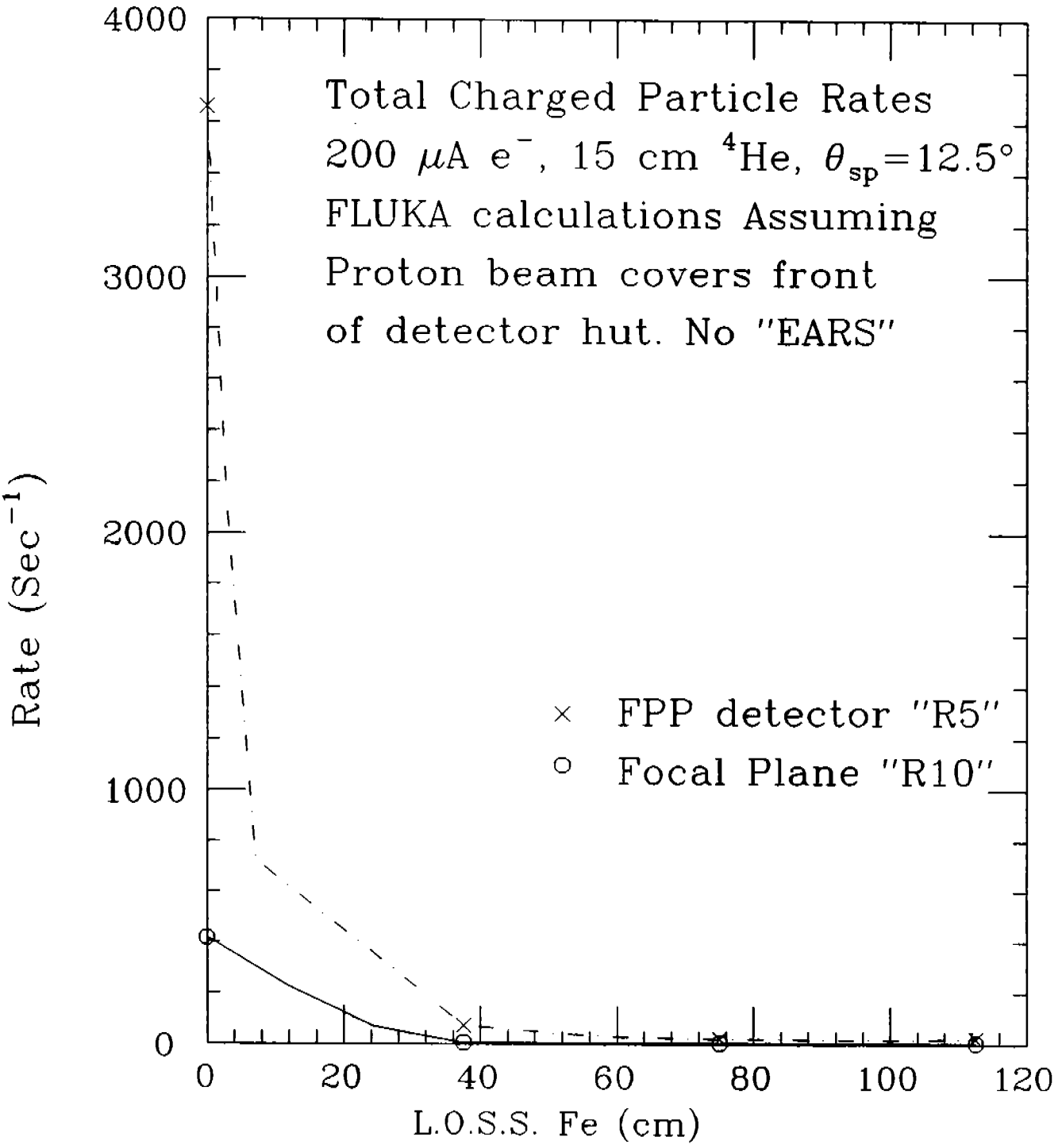
Total Charged Particle Rates
200 μA e⁻, 15 cm ⁴He, θsp=12.5°
FLUKA calculations Assuming
Proton beam covers front
of detector hut. No "EARS"
× FPP detector "R5"
○ Focal Plane "R10"
Rate (Sec⁻¹)
L.O.S.S. Fe (cm)
4000
3000
2000
1000
0
0
20
40
60
80
100
120

Figure 11

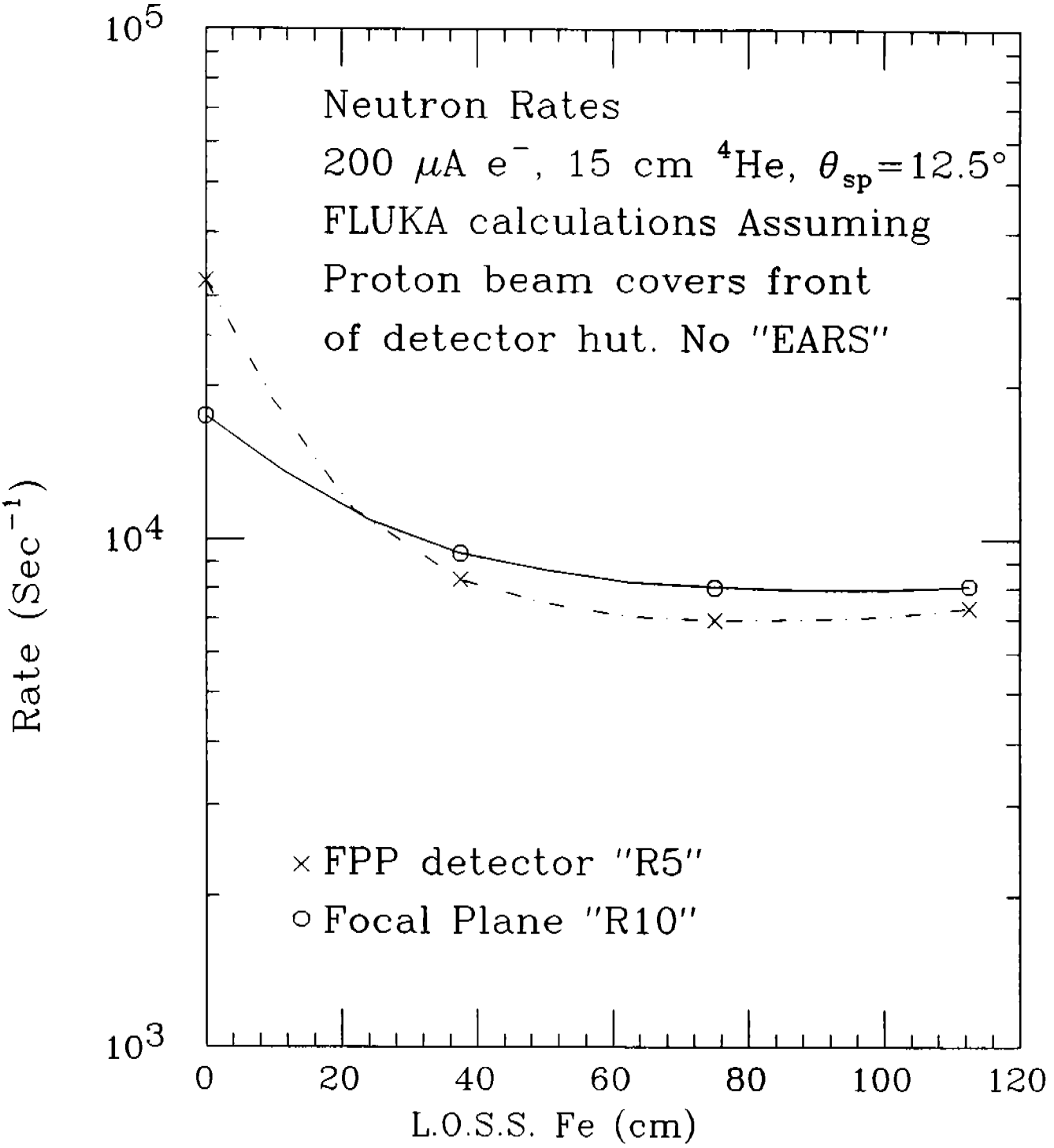
Neutron Rates
200 μA e⁻, 15 cm ⁴He, θsp=12.5°
FLUKA calculations Assuming
Proton beam covers front
of detector hut. No "EARS"
× FPP detector "R5"
○ Focal Plane "R10"
Rate (Sec⁻¹)
10⁵
10⁴
10³
0
20
40
60
80
100
120
L.O.S.S. Fe (cm)

Figure 12

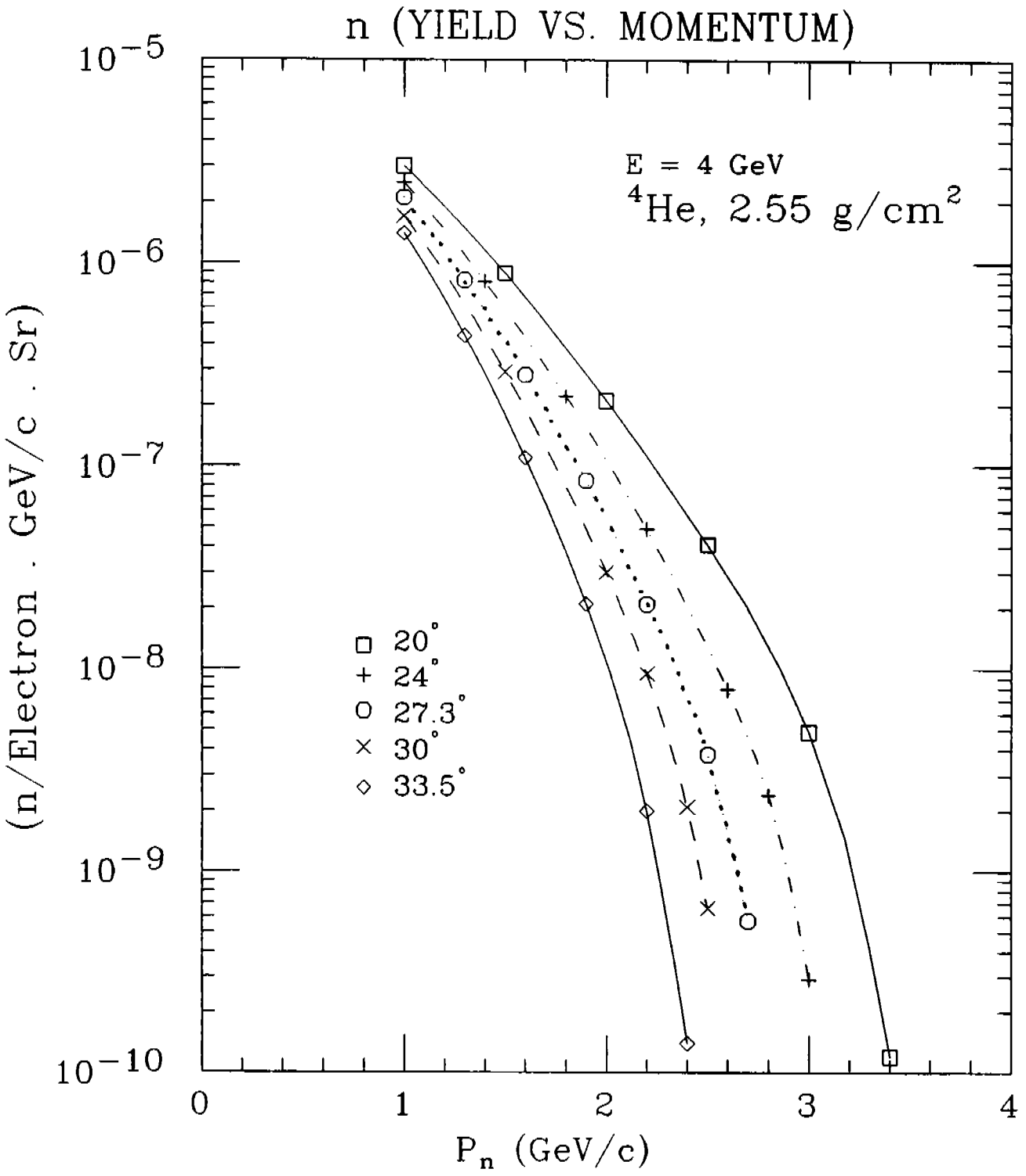
n (YIELD VS. MOMENTUM)
E = 4 GeV
^{4}He, 2.55 g/cm^2
20°
24°
27.3°
30°
33.5°
(n/Electron . GeV/c . Sr)
P_n (GeV/c)
10^{-5}
10^{-6}
10^{-7}
10^{-8}
10^{-9}
10^{-10}
0
1
2
3
4

Figure 13

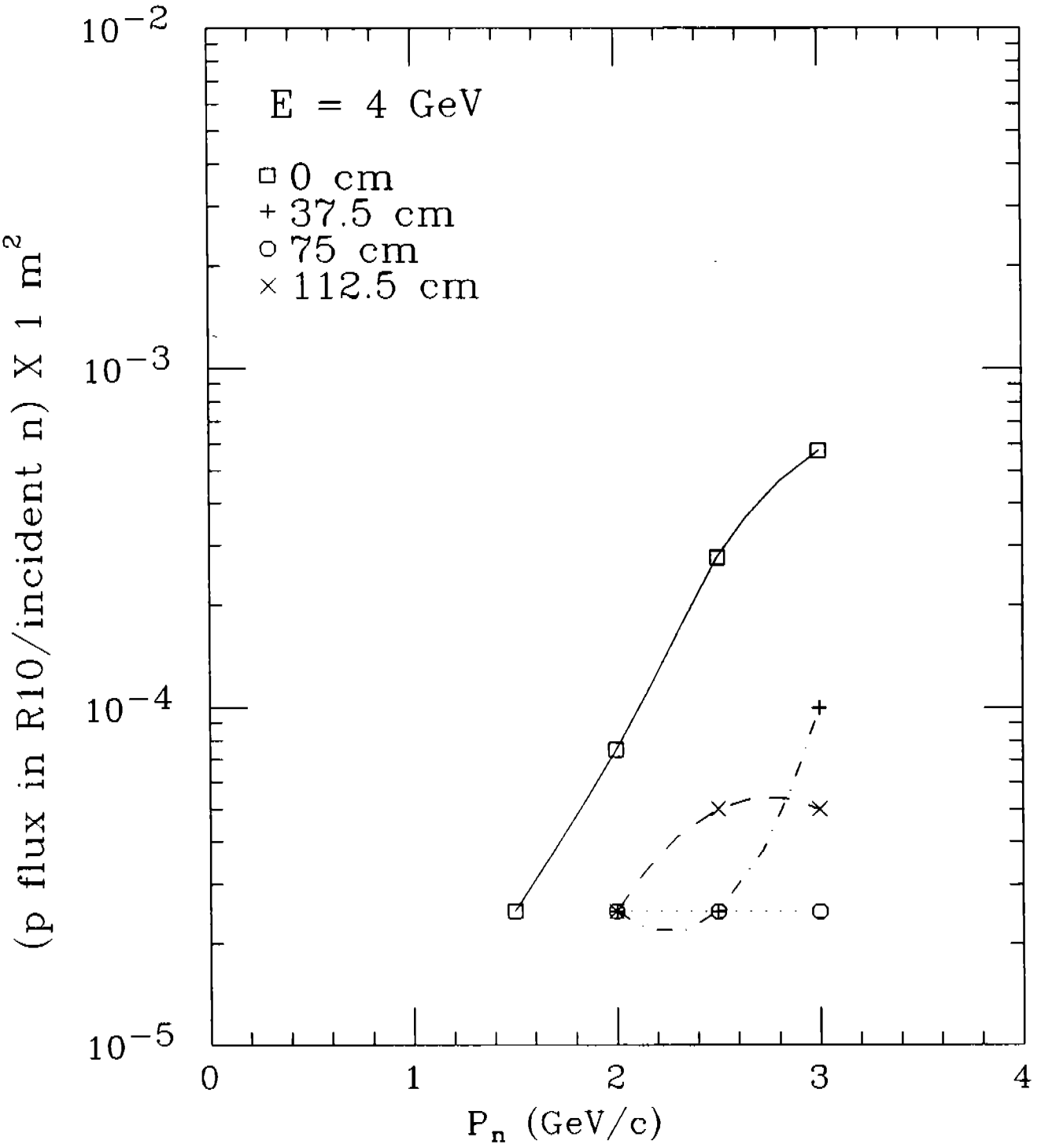
E = 4 GeV
0 cm
37.5 cm
75 cm
112.5 cm
10^{-2}
10^{-3}
10^{-4}
10^{-5}
(p flux in R10/incident n) X 1 m^2
0
1
2
3
4
P_n (GeV/c)

Figure 14

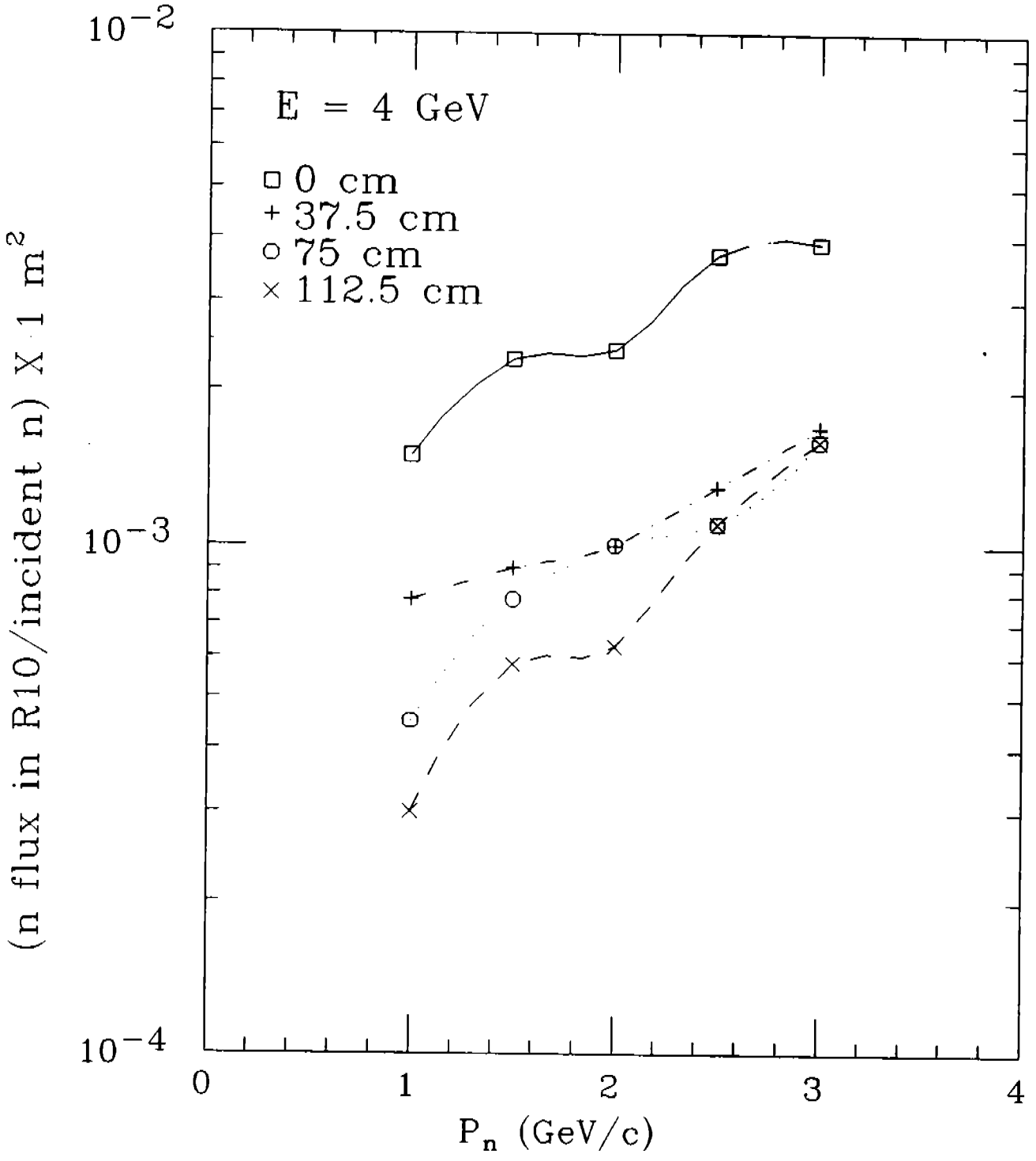
E = 4 GeV
0 cm
37.5 cm
75 cm
112.5 cm
10^{-2}
10^{-3}
10^{-4}
(n flux in R10/incident n) X 1 m^2
0
1
2
3
4
P_n (GeV/c)

Figure 15

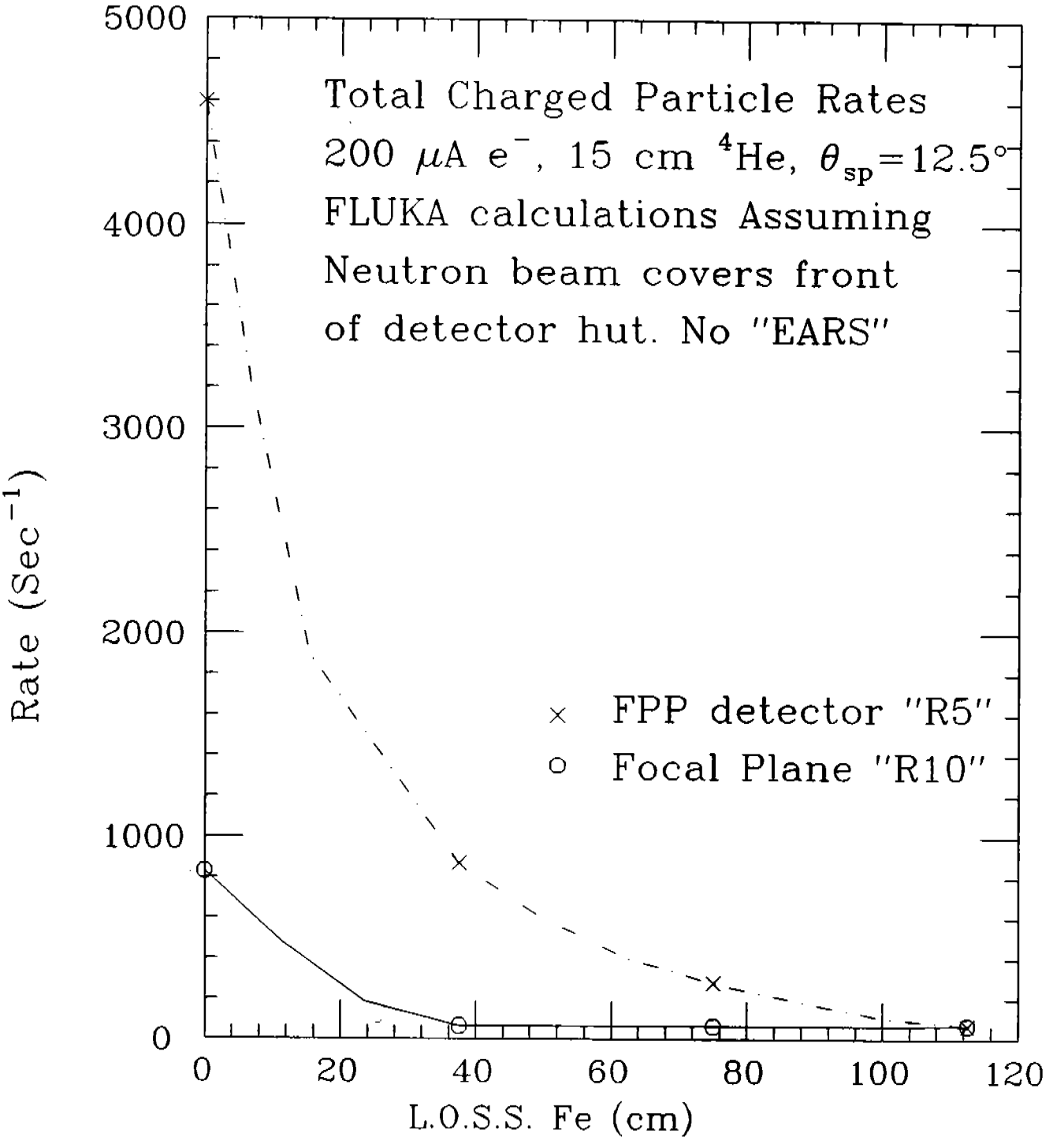
Total Charged Particle Rates
200 μA e⁻, 15 cm ⁴He, θsp=12.5°
FLUKA calculations Assuming
Neutron beam covers front
of detector hut. No "EARS"
× FPP detector "R5"
○ Focal Plane "R10"
Rate (Sec⁻¹)
L.O.S.S. Fe (cm)
0
1000
2000
3000
4000
5000
0
20
40
60
80
100
120

Figure 16

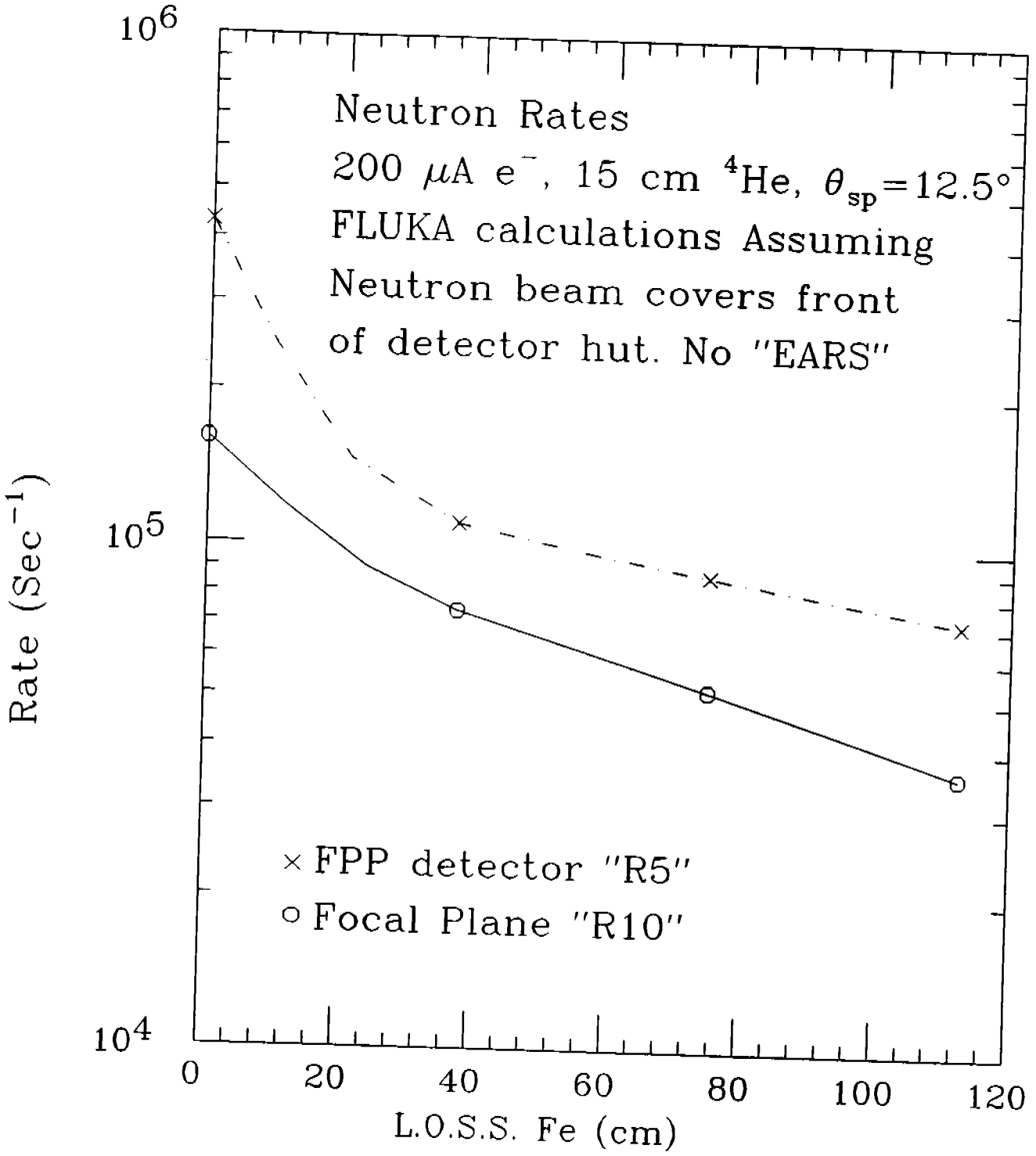
Neutron Rates
200 μA e⁻, 15 cm ⁴He, θsp=12.5°
FLUKA calculations Assuming
Neutron beam covers front
of detector hut. No "EARS"
× FPP detector "R5"
○ Focal Plane "R10"
Rate (Sec⁻¹)
10⁶
10⁵
10⁴
0
20
40
60
80
100
120
L.O.S.S. Fe (cm)

Figure 17